nature immunology

SUPPLEMENTARY INFORMATION

https://doi.org/10.1038/s41590-018-0182-3

In the format provided by the authors and unedited.

Hyperactivated PI3Kδ promotes self and commensal reactivity at the expense of optimal humoral immunity

Silvia Preite[1,2*], Jennifer L. Cannons[1,2,12], Andrea J. Radtke[2,12], Ivan Vujkovic-Cvijin[3,12], Julio Gomez-Rodriguez[1,2], Stefano Volpi[4,5], Bonnie Huang[1,2], Jun Cheng[1], Nicholas Collins[3], Julie Reilley[1,2], Robin Handon[1], Kerry Dobbs[6], Lutfi Huq[3], Indu Raman[7], Chengsong Zhu[7], Quan-Zhen Li[7,8], Ming O. Li[9], Stefania Pittaluga[10], Gulbu Uzel[6], Luigi D. Notarangelo[6], Yasmine Belkaid[3,11], Ronald N. Germain[2] and Pamela L. Schwartzberg[1,2*]

[1]National Human Genome Research Institute, National Institutes of Health, Bethesda, MD, USA. [2]Laboratory of Immune System Biology, National Institute of Allergy and Infectious Diseases, National Institutes of Health, Bethesda, MD, USA. [3]Laboratory of Parasitic Diseases, National Institute of Allergy and Infectious Diseases, National Institutes of Health, Bethesda, MD, USA. [4]Clinica Pediatrica e Reumatologia, Centro per le Malattie Autoinfiammatorie e Immunodeficienze, Istituto Giannina Gaslini, Genoa, Italy. [5]Università degli Studi di Genova, Genoa, Italy. [6]Laboratory of Clinical Immunology and Microbiology, National Institute of Allergy and Infectious Diseases, National Institutes of Health, Bethesda, MD, USA. [7]Microarray Core Facility, University of Texas Southwestern Medical Center, Dallas, TX, USA. [8]Department of Immunology, University of Texas Southwestern Medical Center, Dallas, TX, USA. [9]Immunology Program, Memorial Sloan-Kettering Cancer Center, New York, NY, USA. [10]Laboratory of Pathology, National Cancer Institute, National Institutes of Health, Bethesda, MD, USA. [11]Microbiome Program, National Institute of Allergy and Infectious Diseases, National Institutes of Health, Bethesda, MD, USA. [12]These authors contributed equally to this work: Jennifer L. Cannons, Andrea J. Radtke, Ivan Vujkovic-Cvijin. *e-mail: silvia.preite@nih.gov; pams@mail.nih.gov

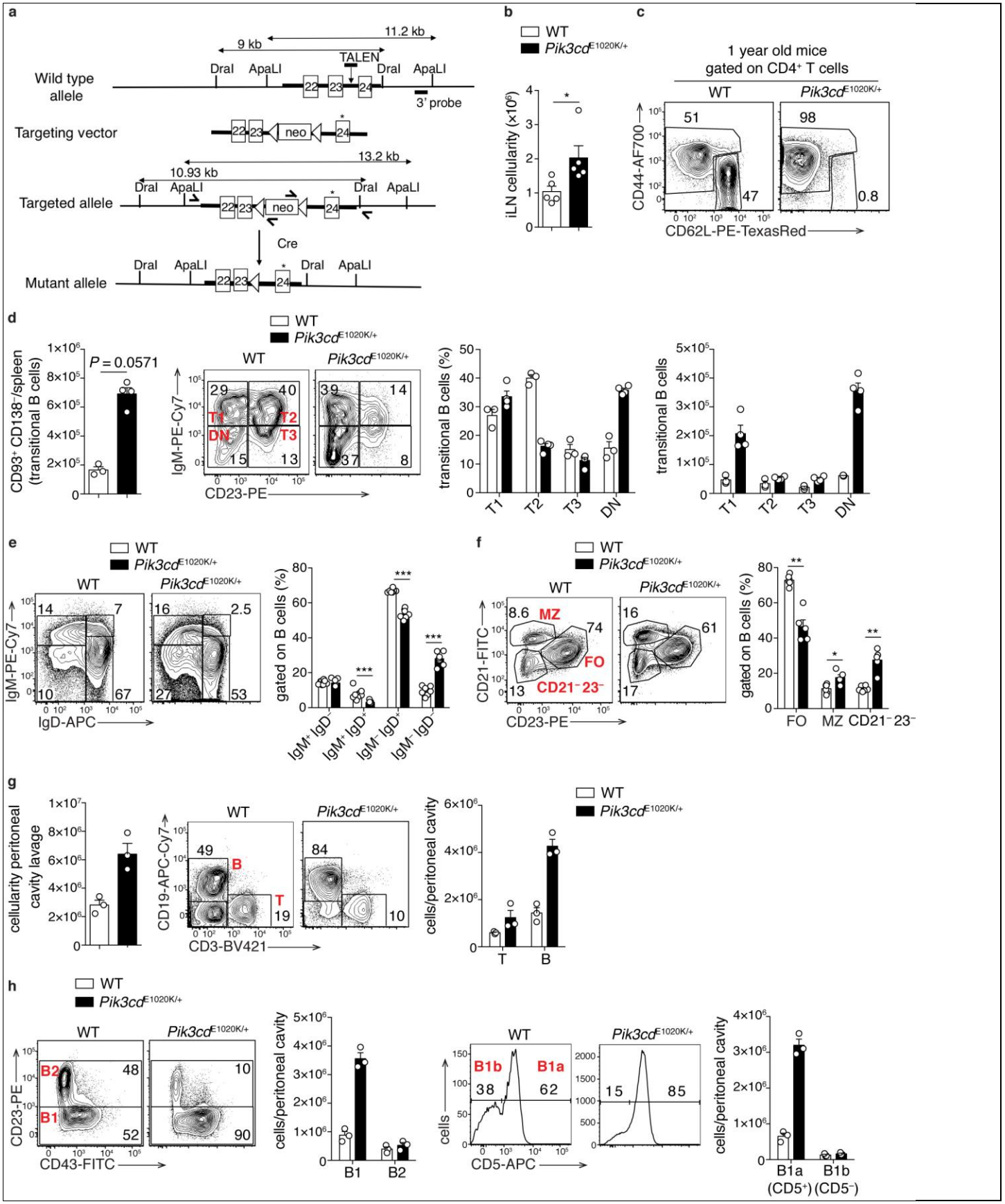
a
11.2 kb
9 kb
TALEN
DraI ApaLI
DraI ApaLI
Wild type allele
22 23 24
3' probe
Targeting vector
neo
13.2 kb
10.93 kb
Targeted allele
Cre
Mutant allele
b
WT
Pik3cd E1020K/+
iLN cellularity (×10⁶)
c
1 year old mice
gated on CD4⁺ T cells
CD44-AF700
CD62L-PE-TexasRed
51
47
98
0.8
d
CD93⁺ CD138⁻/spleen (transitional B cells)
P = 0.0571
IgM-PE-Cy7
CD23-PE
T1
T2
T3
DN
29
40
15
13
39
14
37
8
transitional B cells (%)
transitional B cells
e
IgM-PE-Cy7
IgD-APC
14
7
10
67
16
2.5
27
53
gated on B cells (%)
IgM⁺ IgD⁻
IgM⁺ IgD⁺
IgM⁻ IgD⁺
IgM⁻ IgD⁻
f
CD21-FITC
CD23-PE
8.6
MZ
74
FO
13
CD21⁻ 23⁻
16
61
17
FO
MZ
CD21⁻ 23⁻
g
cellularity peritoneal cavity lavage
CD19-APC-Cy7
CD3-BV421
49
B
T
19
84
10
cells/peritoneal cavity
T
B
h
CD23-PE
CD43-FITC
B2
B1
48
52
10
90
cells/peritoneal cavity
B1
B2
B1b
B1a
38
62
15
85
cells
CD5-APC
B1a (CD5⁺)
B1b (CD5⁻)

Supplementary Figure 1

Basal characterization of *Pik3cd*$^{E1020K/+}$ mouse model.

a, Schematic representation of *Pik3cd*$^{E1020K/+}$ generation. After crossing to ZP3-Cre mice to remove the neoR cassette, the point mutation and one LoxP site in the upstream intron remain. (**b, d-h**) Wild-type and *Pik3cd*$^{E1020K/+}$ mice were analyzed at steady state between 2 and 4 months of age. **b**, Cellularity of resting lymph node (n=5 per group). **c**, Representative contour plots of CD44 and CD62L on CD4^{+} T cells in the spleen of 1-year-old mice. **d**, Numbers of CD93^{+}CD138$^{—}$ transitional B cells in the spleen (percent of B220^{+}CD19^{+}); representative flow staining and histograms of percentages and numbers of T1, T2, T3 and IgM$^{—}$ CD23$^{—}$ B cells (gated on B220^{+}CD19^{+}CD93^{+}CD138$^{—}$) (wild-type n=3, *Pik3cd*$^{E1020K/+}$ n=4). **e**, Representative FACS plots of surface IgM and IgD (gated on B220^{+}CD19^{+} B cells in the spleen) and relative histograms (wild-type n=8 *Pik3cd*$^{E1020K/+}$ n=7). **f**, Illustrative contour plots for CD21 and CD23 to identify MZ, FO, and CD21$^{—}$CD23$^{—}$ B cells in the spleen (percent of B220^{+}CD19^{+}). Bar graph on the right (wild-type n=6, *Pik3cd*$^{E1020K/+}$ n=5). **(g-h)** Analysis of peritoneal cavity (n=3 per group). **g**, Cellularity of peritoneal lavage; representative flow staining and cell counts of CD3^{+} T and CD19^{+} B cells. **h**, Representative contour plots and cell counts of B1 (CD23$^{—}$) and B2 (CD23^{+}) B cells gated on CD19^{+} cells as in (**g**); on the right, representative histograms and numbers of B1a (CD5^{+}) and B1b (CD5$^{—}$) gated on B1 B cells. Data in (**b-f**) are representative of three, and data in (**g,h**) of two, independent experiments. Data are represented as mean ± SEM with each dot indicating one mouse. Significance analyzed by Mann-Whitney U test. **P* < 0.05; ***P* < 0.01; ****P* < 0.001.

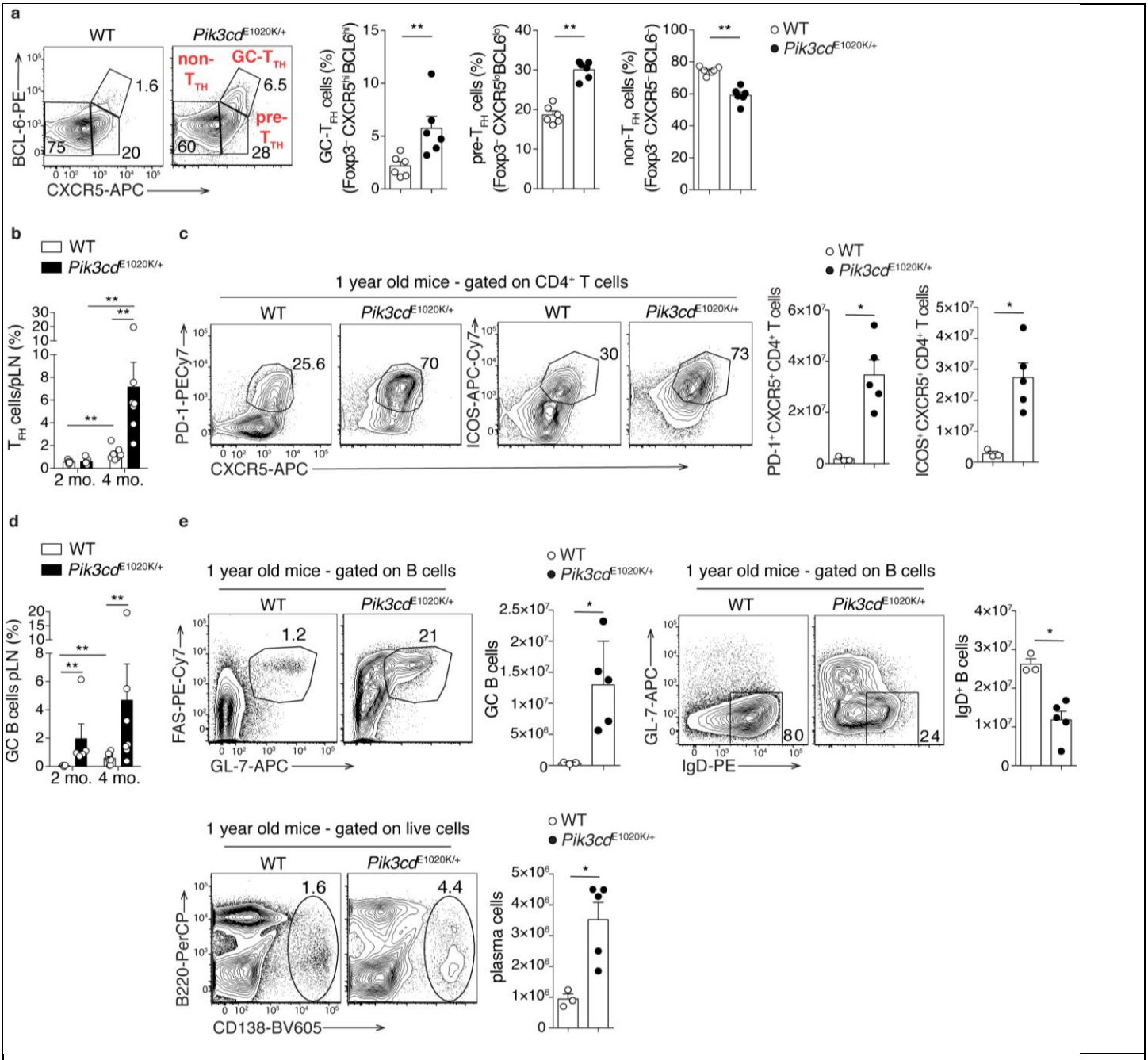

Supplementary Figure 2

Baseline immune response of wild-type and *Pik3cd*$^{E1020K/+}$ mice in lymph node and spleen.

a, Representative flow plots and histogram of BCL-6 and CXCR5 staining for GC-T_{FH}, pre-T_{FH} and non-T_{FH} cells (gated on $CD4^+B220^-$ T cells in the spleen) (n=6 per group). **b**, Frequency of PD-$1^+CXCR5^+Foxp3^-$ T_{FH} cells (percent of $CD4^+B220^-$ T cells) in the popliteal lymph node of 2 and 4-month-old mice at steady state. **c**, Representative flow plots and cell counts of $CD4^+$ follicular T cells: $CXCR5^+PD\text{-}1^+$ (left panel) and $CXCR5^+ICOS^+$ (right panel) in 1-year-old mice in the spleen. **d**, Frequency of GL-7^+FAS^+ GC B cells (percent of $B220^+CD19^+$ B cells) in the popliteal lymph node of 2 and 4-month-old mice at steady state (**b,d**, 2 month-old, n=5 per group; 4 month-old, wild-type n=8, *Pik3cd*$^{E1020K/+}$ n=7). **e**, Representative flow plots and cell counts of GL-7^+FAS^+ GC B cells (percent of $B220^+CD19^+$ B cells, left panel), IgD^+ B cells (percent of $B220^+CD19^+$ B cells, right panel), and $CD138^+B220^{int/lo}$ plasma cells (of live cells, lower panel) in 1-year-old mice in the spleen (**c, e**, wild-type n=3, *Pik3cd*$^{E1020K/+}$ n=5). Data are representative of two independent experiments. Data are represented as mean ± SEM. Significance analyzed by Mann-Whitney U test. *$P < 0.05$; **$P < 0.01$; ***$P < 0.001$.

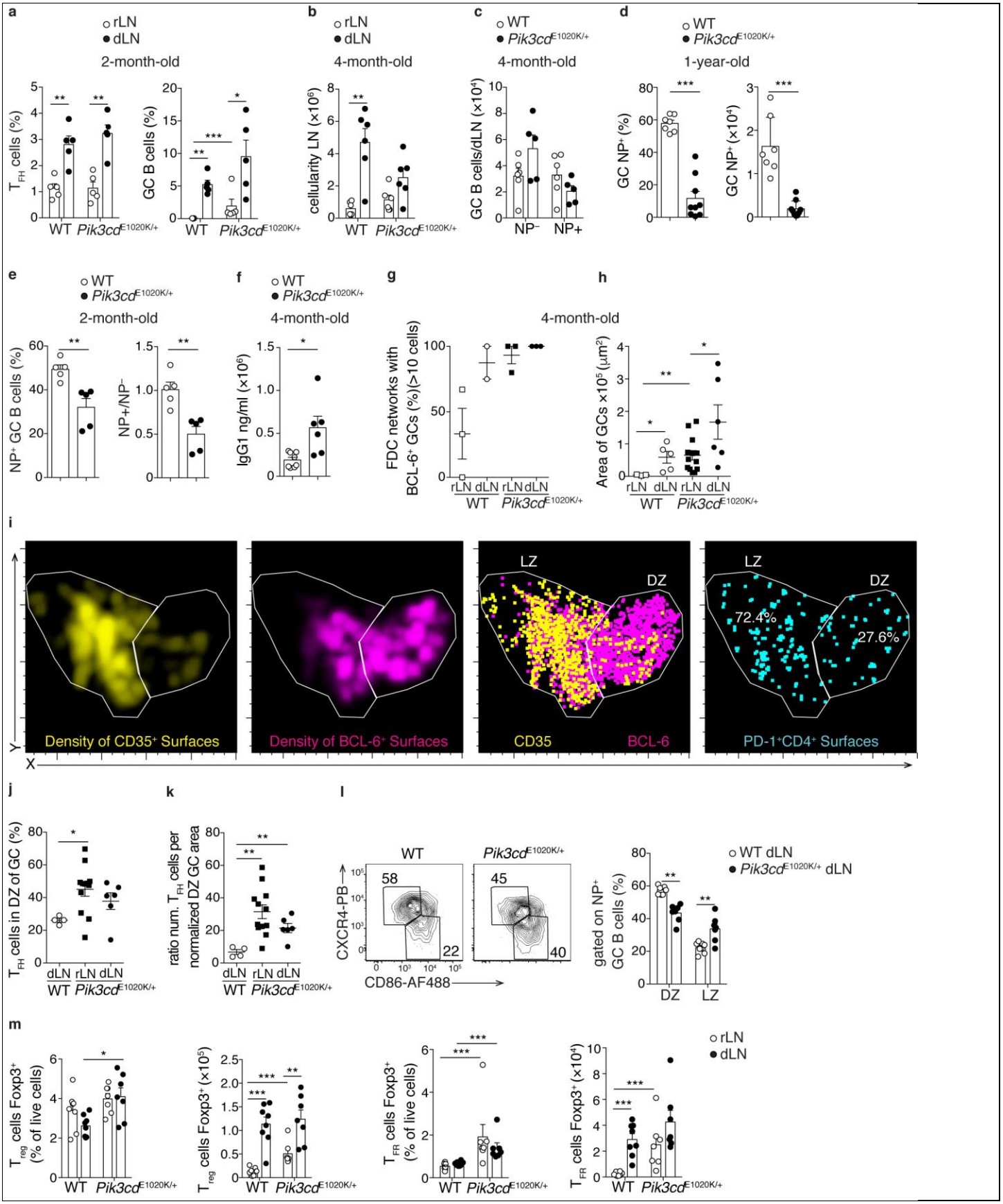
a
rLN
dLN
2-month-old
T_FH cells (%)
GC B cells (%)
WT
Pik3cd^E1020K/+
b
rLN
dLN
4-month-old
cellularity LN (×10^6)
c
WT
Pik3cd^E1020K/+
4-month-old
GC B cells/dLN (×10^4)
NP−
NP+
d
WT
Pik3cd^E1020K/+
1-year-old
GC NP+ (%)
GC NP+ (×10^4)
e
WT
Pik3cd^E1020K/+
2-month-old
NP+ GC B cells (%)
NP+/NP−
f
WT
Pik3cd^E1020K/+
4-month-old
IgG1 ng/ml (×10^6)
g
4-month-old
FDC networks with BCL-6+ GCs (%)(>10 cells)
rLN dLN rLN dLN
WT
Pik3cd^E1020K/+
h
4-month-old
Area of GCs ×10^5 (μm^2)
rLN dLN rLN dLN
WT
Pik3cd^E1020K/+
i
LZ
DZ
72.4%
27.6%
Density of CD35+ Surfaces
Density of BCL-6+ Surfaces
CD35
BCL-6
PD-1+CD4+ Surfaces
Y
X
j
T_FH cells in DZ of GC (%)
dLN rLN dLN
WT
Pik3cd^E1020K/+
k
ratio num. T_FH cells per normalized DZ GC area
dLN rLN dLN
WT
Pik3cd^E1020K/+
l
WT
Pik3cd^E1020K/+
CXCR4-PB
CD86-AF488
58
22
45
40
gated on NP+ GC B cells (%)
DZ
LZ
WT dLN
Pik3cd^E1020K/+ dLN
m
T_reg cells Foxp3+ (% of live cells)
T_reg cells Foxp3+ (×10^5)
T_FR cells Foxp3+ (% of live cells)
T_FR cells Foxp3+ (×10^4)
WT
Pik3cd^E1020K/+
rLN
dLN

Supplementary Figure 3

Immune response to NP-OVA in wild-type and *Pik3cd*$^{E1020K/+}$ mice.

Wild-type and *Pik3cd*$^{E1020K/+}$ mice were immunized subcutaneously, at different age (2-months, 4-months, 1-year-old), with NP-OVA in alum in the hock and sacrificed on day+10. Analyses performed on draining (dLN) and resting (rLN) popliteal lymph nodes. **a**, Analyses of 2-month-old mice: frequency of PD-1^{+}CXCR5^{+}Foxp3^{-} T_{FH} cells (percent of CD4^{+}B220^{-} T cells, left panel) and GL-7^{+}FAS^{+} GC B cells (of B220^{+}CD19^{+} B cells, right panel) in rLN and dLN (n=5 per group). (**b-c**) Analyses of 4-month-old mice. **b**, cellularity of rLN and dLN (n=6 per group). **c**, Numbers of NP^{-} and NP^{+} GC B cells in dLN (wild-type n=6, *Pik3cd*$^{E1020K/+}$ n=5). **d**, Analyses of 1-year-old mice: percentage and numbers of NP^{+} GC B cells in dLN (wild-type n=7, *Pik3cd*$^{E1020K/+}$ n=9). **e**, Analyses of 2-month-old mice: percentage of NP^{+} GC B cells and ratios between numbers of NP^{+} and NP^{-} GC B cells in dLN (n=5 per group). **f**, Analyses of 4-month-old mice: ELISA for serum IgG1 (wild-type n=8, *Pik3cd*$^{E1020K/+}$ n=6). (**g-m**) Analyses based on Figure 3g. **g**, Proportion of FDC networks with a GC having greater than 10 BCL-6^{+} cells (wild-type rLN, n=3; wild-type dLN, n=2; *Pik3cd*$^{E1020K/+}$ rLN and dLN n=3). Each symbol represents an entire LN section corresponding to 5-8 FDC networks. **h**, Area of BCL-6^{+} GCs per FDC region. Each symbol corresponds to a GC (wild-type rLN, n=3; wild-type dLN, n=5; *Pik3cd*$^{E1020K/+}$ rLN, n=13; *Pik3cd*$^{E1020K/+}$ dLN n=6). **i**, Histo-cytometric representation of GCs from wild-type dLN depicted in Figure 3g, II. The distribution of PD-1^{+}CD4^{+} T cells within the LZ and DZ of the GC was determined using the density of CD35 and BCL-6 to mark the LZ and DZ, respectively. **j**, Percentage of T_{FH} cells (PD-1^{+}CD4^{+} surfaces) in the DZ as determined by histo-cytometry. **k**, Normalized numbers of T_{FH} cells (identified as in **j**) per DZ GC area (BCL-6^{+}CD35^{-}). Each symbol corresponds to a GC (**j,k,** wild-type dLN, n=4; *Pik3cd*$^{E1020K/+}$ rLN, n=12; *Pik3cd*$^{E1020K/+}$ dLN n=6). IF analyses are representative of 2-3 independent lymph nodes analyzed. **l**, Representative FACS plots and histograms of DZ (CXCR4^{hi}CD86^{lo}) and LZ (CXCR4^{lo}CD86^{hi}) gated on NP^{+} GC B cells (wild-type n=8, *Pik3cd*$^{E1020K/+}$ n=7). **m**, Percentage (of live cells) and numbers of CD4^{+}B220^{-}CXCR5^{-}PD1^{-} Foxp3^{+} T_{reg} cells, and CD4^{+}B220^{-}PD-1^{+}CXCR5^{+}Foxp3^{+} T_{FR} cells in rLN and dLN (wild-type n=8, *Pik3cd*$^{E1020K/+}$ n=7). Data in (**a-f, l, m**) are representative of two independent experiments. Shown is the mean ± SEM. Significance analyzed by Mann-Whitney U test. *P < 0.05; **P < 0.01; ***P < 0.001.

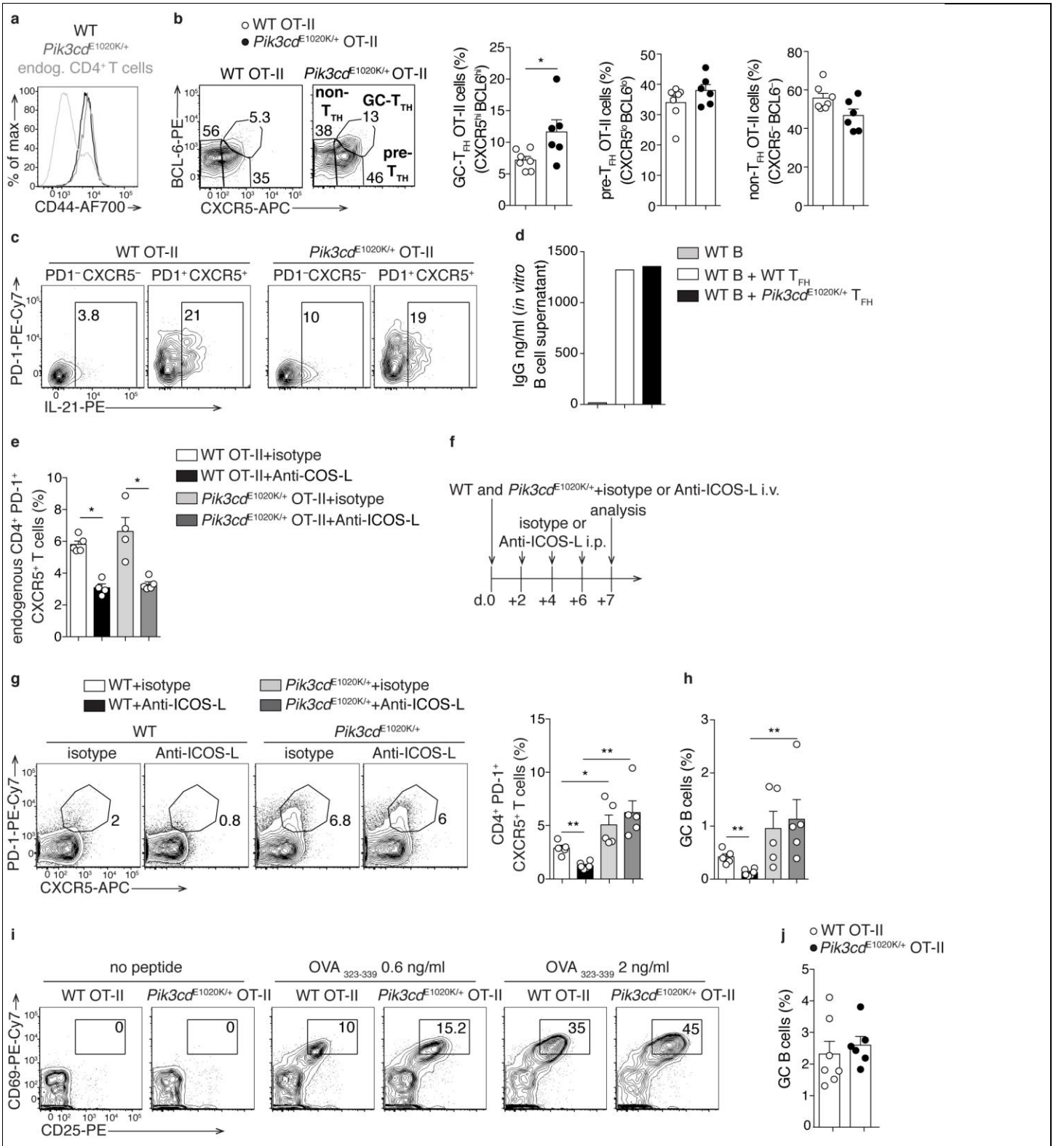

Supplementary Figure 4

T cell intrinsic roles of hyperactivated PI3Kδ.

(a-b, c, j) Experimental setting described in Figure 4a. **a,** Representative CD44 histogram on wild-type and *Pik3cd*$^{E1020K/+}$ OT-II cells

and endogenous $CD4^+$ T cells. **b**, Representative flow plots and histograms of GC-T_{FH}, pre-T_{FH} and non-T_{FH} cells (gated on transferred OT-II cells in the spleen) (wild-type n=7, *Pik3cd*$^{E1020K/+}$ n=6). **c**, Intracellular staining for IL-21 after *in vitro* re-stimulation with PMA/Ionomycin on FACS sorted wild-type or *Pik3cd*$^{E1020K/+}$ OT-II non-T_{FH} cells ($PD1^-CXCR5^-CD4^+B220^-$) and T_{FH} cells ($PD1^+CXCR5^+CD4^+B220^-$), isolated on day +7 post immunization, as described in Fig. 4a (pool of wild-type OT-II (n=7) and *Pik3cd*$^{E1020K/+}$ OT-II cells (n=6)). **d**, Analysis of IgG supernatant on *in vitro* culture between wild-type B cells and wild-type or *Pik3cd*$^{E1020K/+}$ polyclonal T_{FH} cells stimulated with anti-IgM and anti-CD3 for 7 days (pool of 4-5 mice per group). **e**, Frequency of endogenous $PD\text{-}1^+CXCR5^+$ of $CD4^+$ $B220^-$ T cells in wild-type mice adoptively transferred with wild-type or *Pik3cd*$^{E1020K/+}$ OT-II cells and treated with isotype control (wild-type OT-II n=5, *Pik3cd*$^{E1020K/+}$ OT-II n=4), or anti-ICOS-L (wild-type OT-II n=4, *Pik3cd*$^{E1020K/+}$ OT-II n=5) (experiment described in Fig. 4d). **f**, Experiment outline of (**g, h**). Naïve wild-type and *Pik3cd*$^{E1020K/+}$ mice received isotype control (wild-type n=5, *Pik3cd*$^{E1020K/+}$ n=5), or anti-ICOS-L (wild-type n=6, *Pik3cd*$^{E1020K/+}$ n=5) on day 0 (i.v.), +2, +4, +6 (i.p.) and were sacrificed on day+7 post treatment. **g**, Representative contour plots and histogram of endogenous $PD\text{-}1^+CXCR5^+$ T cells (of $CD4^+B220^-$). **h**, Histogram of $FAS^+GL\text{-}7^+$ GC B cells (of $B220^+CD19^+$ B cells). **i**, Analysis of CD69 and CD25 on wild-type and *Pik3cd*$^{E1020K/+}$ naïve OT-II cells activated *in vitro* with $CD11c^+$ DC and $OVA_{323\text{-}339}$ for 20 h (pool of 2-3 mice per group). **j**, Frequency of $FAS^+GL\text{-}7^+$ GC B cells (of $B220^+CD19^+$ B cells) related to Fig. 4a (wild-type n=7, *Pik3cd*$^{E1020K/+}$ n=6). Data are representative of two independent experiments. Data are expressed as mean ± SEM with each dot indicating one mouse. Significance analyzed by Mann-Whitney U test. **P* < 0.05; ***P* < 0.01.

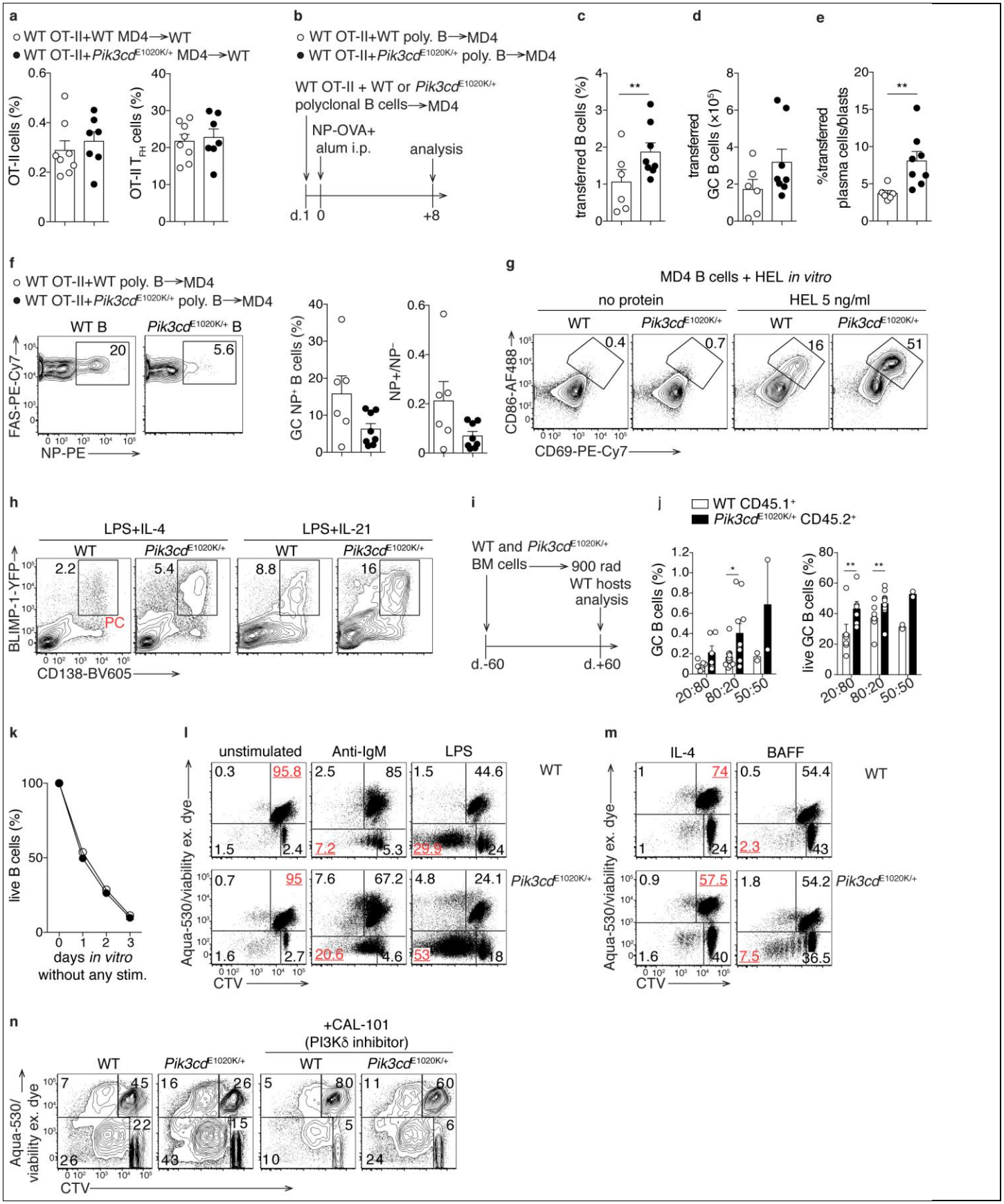
a
WT OT-II+WT MD4→WT
WT OT-II+Pik3cd^E1020K/+ MD4→WT
OT-II cells (%)
OT-II T_FH cells (%)
b
WT OT-II+WT poly. B→MD4
WT OT-II+Pik3cd^E1020K/+ poly. B→MD4
WT OT-II + WT or Pik3cd^E1020K/+ polyclonal B cells→MD4
NP-OVA+ alum i.p.
analysis
d.1 0
+8
c
transferred B cells (%)
d
transferred GC B cells (×10^5)
e
%transferred plasma cells/blasts
f
WT OT-II+WT poly. B→MD4
WT OT-II+Pik3cd^E1020K/+ poly. B→MD4
WT B
Pik3cd^E1020K/+ B
FAS-PE-Cy7
NP-PE
GC NP+ B cells (%)
NP+/NP-
g
MD4 B cells + HEL in vitro
no protein
HEL 5 ng/ml
WT
Pik3cd^E1020K/+
CD86-AF488
CD69-PE-Cy7
h
LPS+IL-4
LPS+IL-21
BLIMP-1-YFP
PC
CD138-BV605
i
WT and Pik3cd^E1020K/+ BM cells
900 rad
WT hosts
analysis
d.-60
d.+60
j
WT CD45.1+
Pik3cd^E1020K/+ CD45.2+
GC B cells (%)
live GC B cells (%)
20:80
80:20
50:50
k
live B cells (%)
days in vitro without any stim.
l
unstimulated
Anti-IgM
LPS
WT
Pik3cd^E1020K/+
Aqua-530/viability ex. dye
CTV
m
IL-4
BAFF
n
+CAL-101
(PI3Kδ inhibitor)

Supplementary Figure 5

B cell intrinsic roles of hyperactivated PI3Kδ.

a, Related to Figure 5a. Frequency of wild-type OT-II and wild-type OT-II T_{FH} cells (PD-1^+CXCR5^+CD4^+B220^-) in wild-type hosts together with wild-type (n=8) or mutant (n=7) MD4 B cells immunized i.p. with HEL-OVA $_{323-339}$ in alum. **b**, Schematic experimental layout for panels (**c-f**). Wild-type OT-II (CD45.1^+) and wild-type (n=6) or *Pik3cd*$^{E1020K/+}$ (n=8) polyclonal B cells (CD45.2^+) were adoptively transferred into MD4 hosts (CD45.1/2^+) and immunized i.p. with NP-OVA in alum. Analysis in the spleen on day+8. **c**, Frequency of transferred polyclonal CD45.2^+B220^+CD19^+ B cells (of live cells). **d**, Numbers of transferred CD45.2^+B220^+CD19^+GL-7^+FAS$^+$ GC B cells. **e**, Frequency of polyclonal CD138^+B$220^{int/lo}$ plasma cells/blasts (of transferred CD45.2^+ cells). **f**, Representative contour plots of frequency of NP$^+$ GC B cells within transferred B cells, histogram of NP$^+$ GC B cells, and ratio between numbers of NP$^+$ and NP$^-$ GC B cells. **g**, Analysis of CD86 and CD69 on wild-type and *Pik3cd*$^{E1020K/+}$ follicular (FO) MD4 B cells activated *in vitro* with HEL for 20 h (pool of 2-3 mice per group). **h**, Analysis of *in vitro* differentiated plasma cells (BLIMP-1-YFP$^+$CD138^+) generated from FO B cells stimulated with LPS and IL-4 or IL-21 for 3 days (gated on live B cells) (pool of 2-3 mice per group). **i**, Experimental outline of mixed BM chimeras between different ratios (20:80 n=6, 80:20 n=10, 50:50 n=2) of wild-type (CD45.1^+) and *Pik3cd*$^{E1020K/+}$ (CD45.2^+) bone marrow cells, transferred into irradiated wild-type hosts (CD45.1/2^+). **j**, Frequency of B220^+CD19^+GL-7^+FAS$^+$ GC B cells within wild-type and *Pik3cd*$^{E1020K/+}$ cells, and live GC B cells (Annexin$^-$ viability dye$^-$). **k**, FO B cells were kept *in vitro* without stimulation and analyzed for viability at different time points (wild-type open circles, mutant closed circles). **l**, **m**, FO B cells were activated *in vitro* for 3 days with the indicated stimuli and assessed for CTV dilution and viability. **n**, FO B cells were stimulated *in vitro* with LPS+IL-4, treated with or without CAL-101 (PI3Kδ inhibitor) and analyzed for CTV dilution and viability on day+3 (**k-n**, pool of 2-3 mice per group). Data are representative of 2 (**a, b-g, i-k, n**), and 3 (**h, l, m**) independent experiments. Data are expressed as mean ± SEM with each dot indicating one mouse. Significance analyzed by Mann-Whitney U test. $^{**}P < 0.01$.

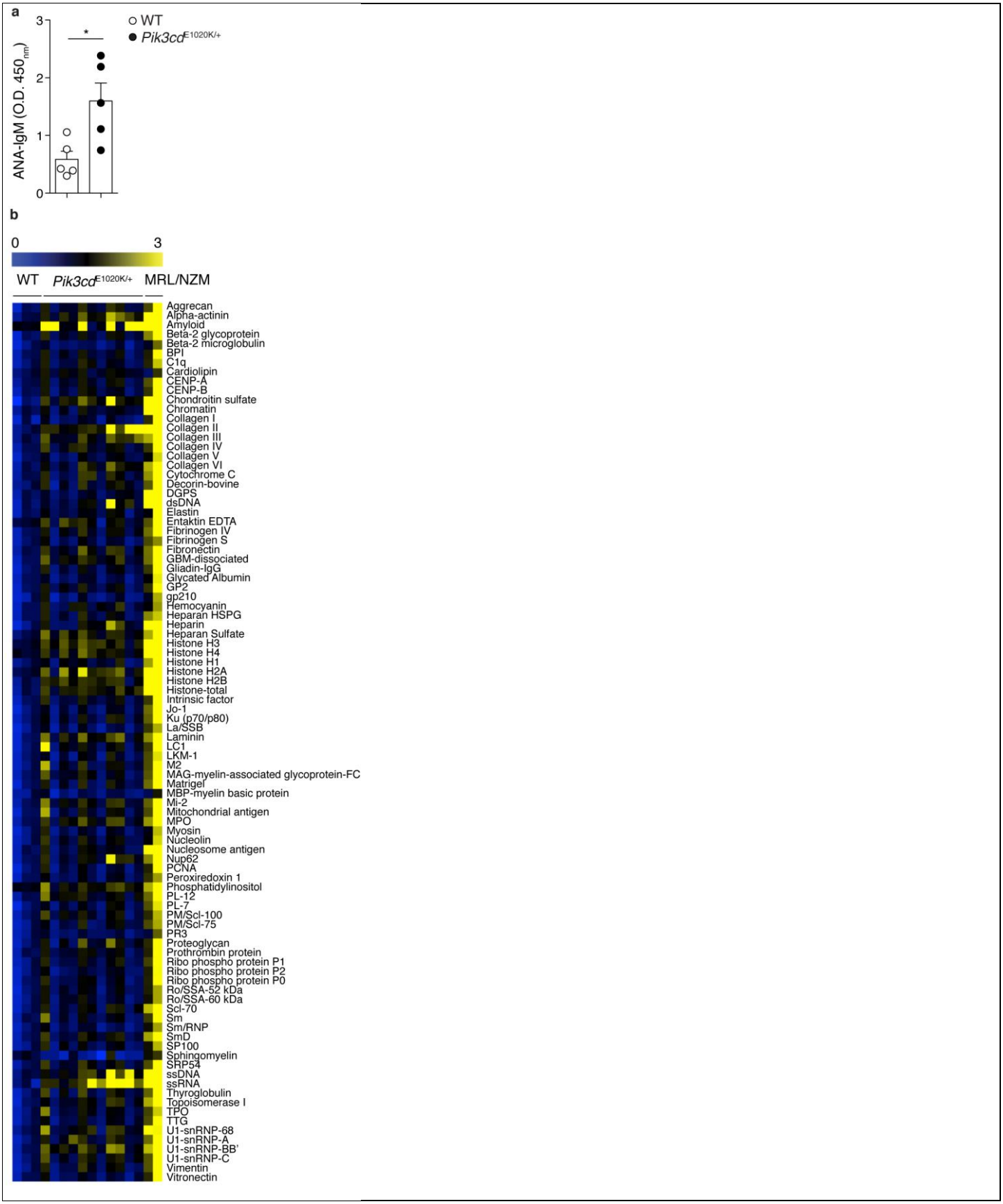
a
ANA-IgM (O.D. 450nm)
WT
Pik3cdE1020K/+
*
b
0
3
WT
Pik3cdE1020K/+
MRL/NZM
Aggrecan
Alpha-actinin
Amyloid
Beta-2 glycoprotein
Beta-2 microglobulin
BPI
C1q
Cardiolipin
CENP-A
CENP-B
Chondroitin sulfate
Chromatin
Collagen I
Collagen II
Collagen III
Collagen IV
Collagen V
Collagen VI
Cytochrome C
Decorin-bovine
DGPS
dsDNA
Elastin
Entaktin EDTA
Fibrinogen IV
Fibrinogen S
Fibronectin
GBM-dissociated
Gliadin-IgG
Glycated Albumin
GP2
gp210
Hemocyanin
Heparan HSPG
Heparin
Heparan Sulfate
Histone H3
Histone H4
Histone H1
Histone H2A
Histone H2B
Histone-total
Intrinsic factor
Jo-1
Ku (p70/p80)
La/SSB
Laminin
LC1
LKM-1
M2
MAG-myelin-associated glycoprotein-FC
Matrigel
MBP-myelin basic protein
Mi-2
Mitochondrial antigen
MPO
Myosin
Nucleolin
Nucleosome antigen
Nup62
PCNA
Peroxiredoxin 1
Phosphatidylinositol
PL-12
PL-7
PM/Scl-100
PM/Scl-75
PR3
Proteoglycan
Prothrombin protein
Ribo phospho protein P1
Ribo phospho protein P2
Ribo phospho protein P0
Ro/SSA-52 kDa
Ro/SSA-60 kDa
Scl-70
Sm
Sm/RNP
SmD
SP100
Sphingomyelin
SRP54
ssDNA
ssRNA
Thyroglobulin
Topoisomerase I
TPO
TTG
U1-snRNP-68
U1-snRNP-A
U1-snRNP-BB'
U1-snRNP-C
Vimentin
Vitronectin

Supplementary Figure 6

Pik3cd$^{E1020K/+}$ mice develop IgM autoantibodies.

(**a-b**) Wild-type and *Pik3cd*$^{E1020K/+}$ sera were analyzed at 14-16 weeks of age. **a**, ELISA for serum ANA-IgM (n=5 per group). **b**, Serum IgM autoantibody array chip is shown; a colorimetric representation of relative autoantibody reactivity in each sample and for each self-antigen is shown based on the scale (0-3) depicted on top of the heat map. The sera of 3 wild-type and 11 *Pik3cd*$^{E1020K/+}$ were analyzed, and sera from 2 lupus-prone MRL/NZM mice were used as a positive control. Data in (**a**) are representative of 2 independent experiments. Data in (**b**) have been obtained from one experiment examining sera from multiple litters. Data are expressed as mean ± SEM with each dot indicating one mouse. Significance analyzed by Mann-Whitney U test. **P* < 0.05.

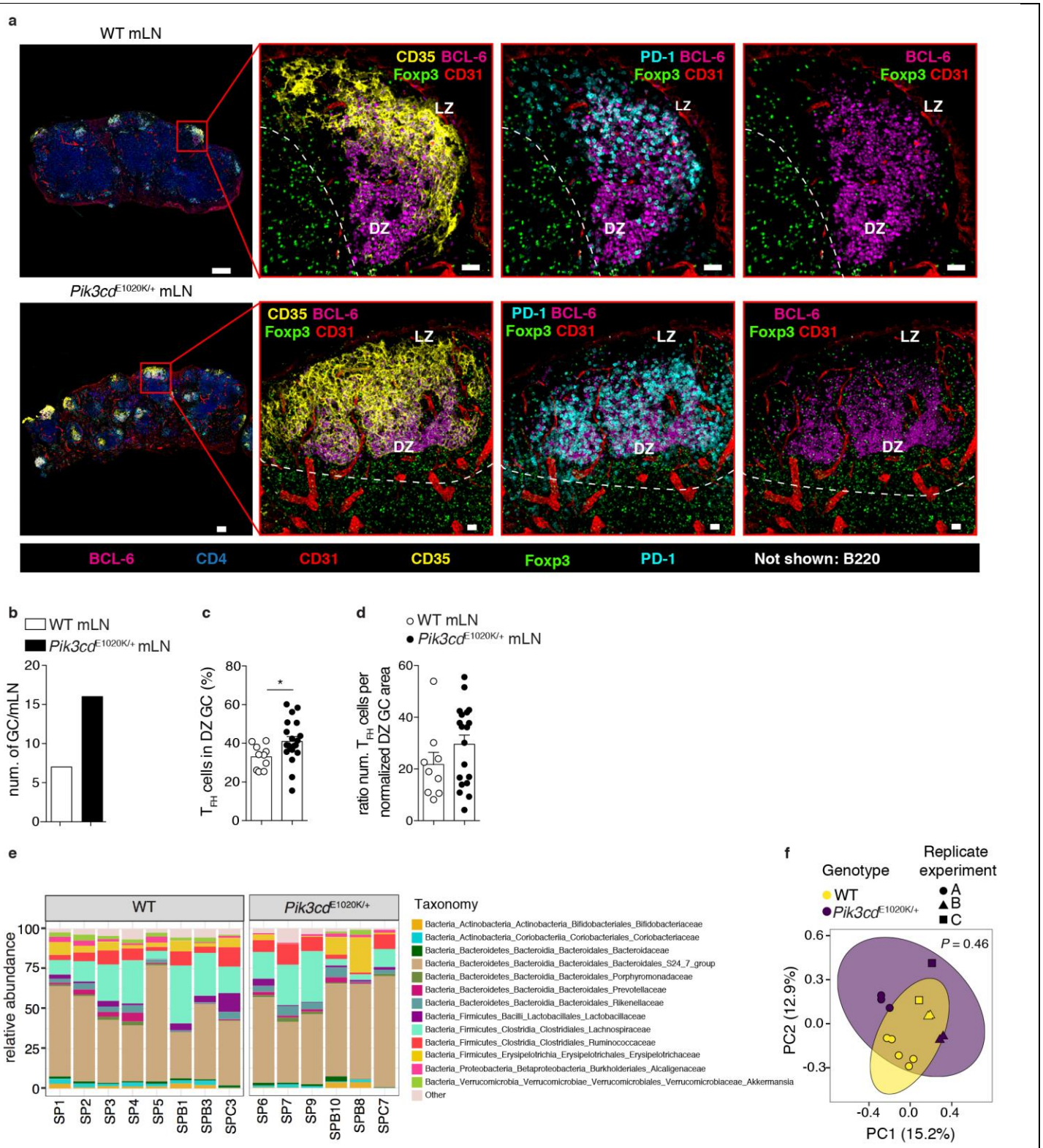

Supplementary Figure 7

Disorganized GCs in *Pik3cd*$^{E1020K/+}$ mLN, and microbiome composition of wild-type and *Pik3cd*$^{E1020K/+}$ mice.

a, Confocal immunofluorescence images from the mLNs of naïve wild-type and *Pik3cd*$^{E1020K/+}$ mice (scale bar 200 μm left panel; 30 μm

enlargements). White dotted line denotes the boundary between the B cell follicle and T cell zone and is based on B220 staining (not shown). CD35 staining intensity was used to mark the light zones (LZ) and dark zones (DZ) of the GC (BCL-6^+). Images are representative of mLNs from 2 mice per group from 2 separate experiments. **b**, Numbers of GCs per mLN (n=1 per group). **c**, Histocytometry was used to quantity the distribution of T_{FH} cells in DZ as described in Supplementary Figure 3f. The percentage of cells within the DZ gate is shown. Each symbol refers to a GC. **d**, Normalized numbers of T_{FH} cells (identified as in **c**) per DZ GC area (BCL-6^+ $CD35^-$) (**c, d,** wild-type n=9, *Pik3cd*$^{E1020K/+}$ n=19) **e**, Bar plots of baseline microbiota profile by 16s rRNA sequencing in wild-type (n=8) and *Pik3cd*$^{E1020K/+}$ (n=6). Relative family-level abundances of fecal samples prior to sorting based on IgA are shown. **f**, Principal Coordinates Analysis (PCoA) plot shown using the Canberra beta diversity metric, performed on baseline microbiota profiles (wild-type n=8; *Pik3cd*$^{E1020K/+}$, n=6). Significance of clustering based on genotype (wild-type vs. *Pik3cd*$^{E1020K/+}$ mice) was assessed using PERMANOVA (P=0.46). Data in (**e, f**) have been obtained from 3 independent experiments. Shown is the mean ± SEM. Differences between groups were compared with Mann-Whitney *U* test. **P* < 0.05.